Effect of CO_2-based binary mixtures on the performance of radial-inflow turbines for the supercritical CO_2 cycles

Yang, Yueming; Wang, Xurong; Hooman, Kamel; Han, Kuihua; Xu, Jinliang; He, Suoying; Qi, Jianhui

DOI
10.1016/j.energy.2022.126429

Publication date
2023

Document Version
Final published version

Published in
Energy

Energy 266 (2023) 126429

Contents lists available at ScienceDirect

Energy

journal homepage: www.elsevier.com/locate/energy

Effect of CO_2-based binary mixtures on the performance of radial-inflow turbines for the supercritical CO_2 cycles

Yueming Yang [a], Xurong Wang [b], Kamel Hooman [c], Kuihua Han [a], Jinliang Xu [d], Suoying He [a], Jianhui Qi [a,d,e,*]

[a] School of Energy and Power Engineering, Shandong University, Jinan 250061, China
[b] School of Energy and Building Environmental Engineering, Henan University of Urban Construction, Pingdingshan 467036, China
[c] Process and Energy Department, Delft University of Technology, 2628 CB, Delft, The Netherlands
[d] Beijing Key Laboratory of Multiphase Flow and Heat Transfer for Low Grade Energy Utilization, North China Electric Power University, Beijing 102206, China
[e] Suzhou Research Institute, Shandong University, Suzhou 215123, China

ARTICLE INFO

Keywords:
Supercritical carbon dioxide
Radial-inflow turbine
CO_2-based binary mixture
Numerical simulation
Turbine stage losses

ABSTRACT

Recently, the supercritical carbon dioxide (SCO_2) power cycle has become a hotspot in the field of energy-efficient utilization. The utilization of additives in the power cycle has been proven to be an effective way to improve the SCO_2 power cycle efficiency. As one of the core components of the system, the influence of CO_2-based mixtures on turbine performance needs to be further explored. In this study, the preliminary design and three-dimensional numerical simulation of a 500 kW radial-inflow turbine (RIT) for small-scale SCO_2 power systems were carried out. Furthermore, the design and off-design performance of high Reynolds number and small size turbine under the change of the CO_2-based binary mixture compositions and mixing ratios were studied. Increasing the amount of nitrogen, oxygen, or helium into CO_2 has a negative effect on the RIT performance, and the appropriate amount of xenon or krypton can improve the turbine efficiency. Moreover, mixtures with higher krypton additions adapt to higher heat source conditions. The loss of the turbine stage passage shows that a large amount of helium greatly reduces the working fluid density, and the high amount of xenon has a great influence on the dynamic viscosity, which all makes the RIT operation deviate from the steady state. Therefore, the CFD model simulation fails indicating that RIT designed based on pure CO_2 may not run smoothly and continuously. The losses in the stage with pure CO_2 and CO_2–Kr mixture were investigated. The results indicate that the losses originated from the stator cannot be ignored and that the improvement of efficiency is mainly owed to the reduction in clearance losses. There is no doubt that the viewpoints proposed in this paper have significant reference value for the practical application of the SCO_2 power cycle using mixtures.

1. Introduction

Demand for low-carbon energy resources has reached a new peak as global efforts to mitigate climate change by reducing carbon emissions [1]. Meanwhile, the energy-saving, high-performance, and safe energy conversion system has always been at the leading edge of research. As an indispensable subsystem of thermal energy conversion, the power cycle module determines the efficiency of the whole system. Selecting an appropriate power cycle module can make low-carbon energy more flexibly applied to the multi-energy distributed architecture system. This system refers to a regional energy internet that can contain a variety of energy resource inputs and has a variety of output functions and transport forms. Considering the limited potential for improving the conversion efficiency of conventional power cycles, innovating the cycle module is necessary. The supercritical carbon dioxide (SCO_2) cycle has attracted extensive attention due to its simple layout, compact system, and high cycle efficiency [2–4], and was first proposed by Feher [5] in 1968.

The SCO_2 power cycle overcomes some limitations of the steam Rankine cycle, such as the large energy input in the compression process, the large heat transfer surfaces, and the large volume of turbomachinery. Moreover, it utilizes the liquid-like properties (the specific volume and compression coefficient are significantly lower than those in the gas phase) near the critical point of the working fluid to reduce the compressor power consumption. However, while simple cycles benefit from the reduced compression work, their efficiency is

* Corresponding author at: School of Energy and Power Engineering, Shandong University, Jinan 250061, China.
E-mail address: j.qi@sdu.edu.cn (J. Qi).

https://doi.org/10.1016/j.energy.2022.126429
Received 2 July 2022; Received in revised form 9 November 2022; Accepted 12 December 2022
Available online 19 December 2022
0360-5442/

Nomenclature

Acronyms

1D	One-dimensional.
3D	Three-dimensional.
N_2	Nitrogen.
O_2	Oxygen.
CFD	Computational fluid dynamics.
CSP	Concentrated solar power.
DES	Distributed energy system
EoS	Equations of state.
He	Helium.
HTR	High temperature recuperator.
Kr	Krypton.
LTR	Low temperature recuperator.
NIST	National Institute of Standards and Technology.
Re	Reynolds number.
RGP	Real gas property.
RIT	Radial-inflow turbine.
SCO_2	Supercritical carbon dioxide.
SMR	Small modular reactors.
Xe	Xenon.

Greek Symbols

α	Absolute flow angle, [°]
β	Relative flow angle, [°]
Δ	Difference, [–].
η	Efficiency, [%]
γ	Isentropic exponent, [–].
μ	Dynamic viscosity, [μPa s].
ρ	Flow density, [kg/m^3].
ϵ	Tip clearance. [mm].

Roman Symbols

$\dot{m}$	Mass flow rate, [kg/s].
h	Enthalpy, [J/kg].
M	Torque, [N m]
P	Pressure, [MPa]
s	Entropy, [J/(kg K)].
T	Temperature, [K]
W	Shaft power, [W]
Z	Blade number, [–].

Subscripts

0	Reference state point.
1,2, …	Number or state point.
g	Working fluid.
s	Isentropic process.
tur	Turbine.

damaged by the significant loss caused by irreversible heat transfer. Angelino [6] also pointed this out, and proposed to construct different cycle layouts to reduce the irreversibility in heat recuperation. A series of later studies on system configuration and layout optimization have also laid the foundation for the application of the SCO_2 cycle [7–9]. Thus, it is vital to choose a suitable power cycle configuration for a given heat source to increase the efficiency of the power cycle.

Currently, researchers are still attempting to improve the efficiency of the SCO_2 power cycle. As we know, cycle efficiency is determined by the temperature and pressure of the high-temperature heat source and the low-temperature heat source. Usually, we try to increase the temperature and pressure of the high-temperature heat source, i.e. the turbine inlet properties. But this way will be limited by the materials of the cycle. Another way is to lower the minimum operating temperature. However, the lowest-temperature point of SCO_2 power cycle is before the inlet of the compressor, which should be slightly above the CO_2 critical temperature (31.6 °C) to guarantee the high cycle efficiency and to avoid condensation of CO_2. This requirement limits the potential of SCO_2 power cycle, as the surrounding temperatures are not always coincident with the CO_2 critical points. Hence, the researcher tries to break the constraints of the physical properties of the CO_2 by shifting the critical point of the CO_2. One possible way is to add other gas, such as N_2, O_2, He, etc., into CO_2 to alter the critical point. This inspires the researchers starting to explore new CO_2-based mixtures, which can be potentially used as the working fluid of the SCO_2 power cycle.

To better understand the effect of different additives on the SCO_2 cycle efficiency, understanding of CO_2 critical point mobility is essential. Jeong et al. [10,11] addressed that the change direction and range of the CO_2 critical point depends on the composition and quantity of additives, such as the addition of helium will decrease the critical temperature. When helium, xenon, and krypton are used as additives, the cycle efficiency under specific operating conditions will be improved due to the increase in cycle temperature range and pressure ratio. What is more, they also proposed that the cycle layouts are crucial to the selection of additives. According to Hu et al. [12], both CO_2–He and CO_2–Kr mixtures can improve the thermodynamic performance of the SCO_2 cycle by increasing cycle efficiency and reducing heat transfer in HTR (high-temperature recuperator) and LTR (low-temperature recuperator). However, in the study of Vesely et al. [13,14], for some cycle layouts, helium showed negative effects like most additives, which confirms Jeong's assertion. Guo et al. [15] carried out a multi-objective optimization in the process of cycle optimization. They recommended that a medium cooling SCO_2–Xe cycle should be adopted for the concentrated solar power (CSP) system, as it has good compatibility to the large specific power in the thermal storage. On the other hand, some solar power plants are located in arid regions and high-temperature areas where the efficiency of the SCO_2 power cycle system is reduced. This is due to the environmental temperature being higher than the critical temperature, and the working fluid cannot be cooled down to the adjacent region of the critical point. Therefore, specific additives are selected to increase the critical temperature of working fluids, which is proved to be effective in improving the system benefit in arid regions. Bonalumi et al. [16] used CO_2-$TiCl_4$ mixtures for solar applications with high-temperature heat sinks. After adding an appropriate amount of $TiCl_4$, the mixture reached a higher critical temperature, resulting in efficiency gains of up to 5% and 3% in the simple cycle and the recompression cycle, respectively. According to Crespi et al. [17], when the mole fractions of $TiCl_4$ and C_6F_6 were between 10% and 25%, the cycle thermal efficiency could reach more than 50% even in the application of CSP energy systems with ambient temperature up to 50°C. Hu et al. [12] also indicated that CO_2-cyclohexane and CO_2-butane mixtures can be applied to Brayton cycles in arid regions or power conversion cycles with higher heat sink temperatures.

The SCARABEUS project funded by the EU's Horizon 2020 research is studying the use of CO_2-based mixtures in optimizing the operating range of supercritical fluid, aiming to improve the operation efficiency and reduce the cost of CSP plants. According to the project, the mixture can broaden the supercritical cycle to the transcritical cycle, resulting in the ability to compress the working fluid in the liquid phase using a pump instead of a compressor, and simplify cycle configuration depending on the chosen mixture composition. Moreover, the air-cooled condenser can obtain high cycle efficiency, especially for

typical CSP plants in high-temperature and arid environments. CO_2-C_6F_6, as an intensively investigated working fluid in the SCARABEUS project, obtains a transcritical cycle with high cycle efficiency when coupled with a solar tower [18]. Some of the above-mentioned additives are organic compounds, such as C_6F_6, butane, and cyclohexane. Invernizzi et al. [19] suggested that the feasibility range of system operating temperatures should take into account the thermal stability of organic compounds. In summary, the CO_2-based mixture concept overcomes some limitations of the conventional SCO_2 power cycles, and the mixture types can be tailored according to the specific boundary conditions of each energy generation plant. Undoubtedly, the CO_2-based mixture concept has great development potential and broad application prospects.

Another possible direction for SCO_2 power cycle utilization is on distributed energy systems (DESs). In recent years, the research on small DESs, especially Small Modular Reactors (SMR), has gradually become a hotspot. In contrary technical direction to the conventional nuclear power plant, i.e. tries to increase the power capacity of the reactor, SMR tries to increase the mobility and flexibility of the reactor. For example, CLEAR-I (China Lead-based Research Reactor), as a mobile advanced nuclear energy system, has ultra-safe, ultra-small, and ultra-long-term technical characteristics, and uses a particular kind of liquid metal (lead, bismuth, lithium, etc.) as the cooling medium [20]. These abilities require applications of the advanced small-scale power cycle, which the SCO_2-based mixtures power cycle illustrates their potential. As the requirements of SMR in DES, the power cycle capacity about kilowatt to megawatt are within the interest of researchers.

The previous study [21] addressed that for small-scale power cycle (less than 20 MW), the radial inflow turbines (RITs) are the most suitable turbomachinery type. RITs work at high temperature, high pressure, and high energy density, which makes their aerodynamic and structure integrative design always the focus of research [22,23]. The performance of RITs will greatly affect the whole cycle efficiency, hence, lots of research are focused on the performance estimation of the RITs. Allison et al. [24] compared the efficiencies for a high-parameter simple Brayton cycle concerning a range of compressor and turbine efficiencies. The results show that every 2% increase in turbine efficiency results in nearly a 1% increase in cycle efficiency, while the influence of compressor efficiency is approximately half. Similarly, Cho et al. [25] pointed out that turbine efficiency has more effect on overall thermal efficiency. Therefore, as the core rotating component of the cycle, the turbines must be selected and designed carefully to reach an exceptional performance. However, those studies are almost using purely CO_2 as working fluids, and the influence of mixtures is hardly revealed. The application of mixtures at the system level has been studied in-depth, but the effect on system components has not been thoroughly explored, especially in turbomachinery. Many studies [11,12,14] have analyzed the cycle efficiency fluctuations caused by the change of the mixture's physical properties from the perspective of thermodynamics. However, their research is under a hypothesis that the turbine efficiency will remain the designed value when adding additives into the working fluids. It is not clear whether the internal flow field of turbomachinery changes significantly with the variation of the mixture's composition and mixing ratio, and whether the performance changes as previously calculated in the cycle optimization. What is more, the lack of design procedures for CO_2-based mixture turbines will also distract the attention of researchers. If we plan to study the mixture's influence on the existing power cycle, a fixed turbine model will be considered. Therefore, this paper adopts a specific turbine geometry model to carry out mixture-related research.

Based on the above-mentioned discussion, the objective of this paper is twofold. Firstly, The influence of mixtures on the power output and isentropic efficiency of the turbine is explored. Though there are no specific design procedures for CO_2-based mixture turbines, this study also evaluated the suitability of SCO_2 turbine operating with CO_2-based mixture, i.e. should it be replaced or optimized with the change of working fluids. Second, the internal flow fields of the turbine based on the pure CO_2 and mixtures are analyzed and compared to reveal the possible reasons for large losses.

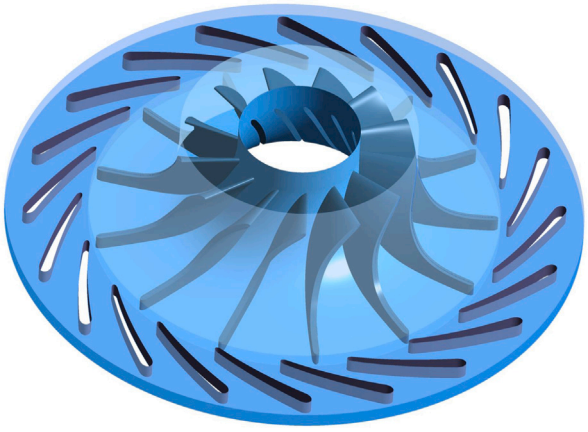

Fig. 1. 3D geometric model of the 500 kW SCO_2 RIT.

This paper is constructed with the following sections. Section 2 describes the model construction and verifies the mesh and mixture properties. Section 3 analyzes the performance and losses when the turbine is operating with mixtures. Finally, Section 4 gives three conclusions and some future works.

2. Methodology

This paper seeks various binary mixtures consisting of CO_2 and oxygen, nitrogen, helium, xenon, or krypton. These additives can be infiltrated impurities such as oxygen and nitrogen or specific substances added to improve the cycle efficiency, such as helium, xenon, and krypton [10,11]. As inert gases, helium, krypton, and xenon also have no impact on the stability of CO_2 at high temperature and pressure. The real gas property (RGP) files for the binary mixtures are obtained by calling the property data of the REFPROP database [26] with an in-house Python code.

To explore the influence of CO_2-based binary mixtures with different components and mixing ratios on the performance of RITs, an efficient computational fluid dynamics (CFD) numerical calculation platform is used to achieve high-precision process simulation.

Details about the methodologies will be discussed in the following sections.

2.1. SCO_2 radial-inflow turbine model

To build a power cycle test-rig suitable for an SMR in DESs, a small-scale power turbine test platform is necessary. Moreover, the RIT's design can be scaled while maintaining the same aerodynamic flows and performance by using the specific speed parameter (N_s) [21]. Therefore, different RITs can match the kilowatt-level or megawatt-level power generation systems through scaling up, which can be flexibly applied to movable nuclear power plants. Finally, a 500 kW SCO_2 RIT is selected and generated. This turbine, with very high speed without exceeding the bearing range, can be used as a representative of SCO_2 RITs used in small DESs. The stator and rotor geometry of the turbine are generated by using the preliminary design tool TOPGEN [21,27], as shown in Fig. 1.

TOPGEN is a University of Queensland in-house code for RITs developed by the Queensland Geothermal Energy Centre of Excellence. This in-house code includes the calculation of flow and geometric features for both the stator and rotor. An iterative calculation process for each combination of head and flow coefficients with rotational speed is

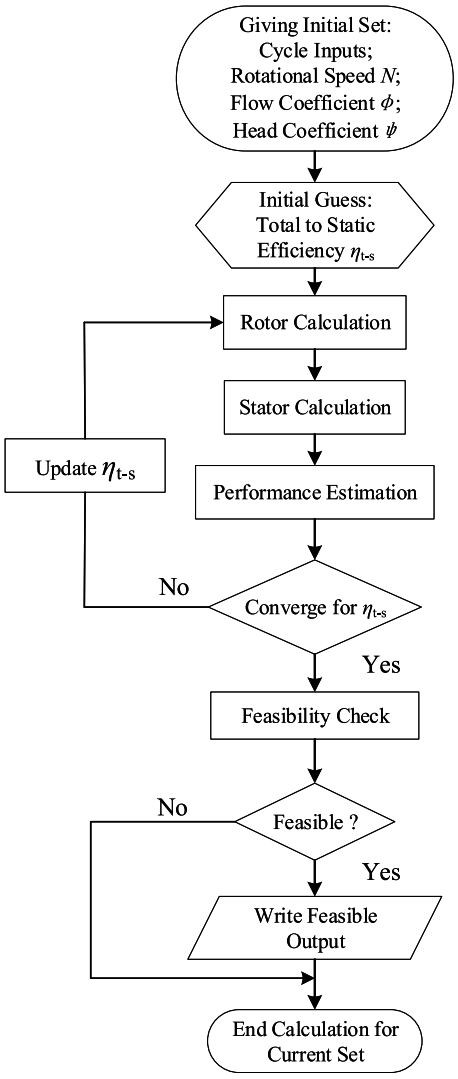

Fig. 2. An overview of the TOPGEN calculation process [27].

illustrated in Fig. 2. The rotor design part takes into account the well-established loss model to estimate the total losses. For the stator design process, TOPGEN does not consider the loss and assumes it as an isentropic expansion process [27]. However, in the research process, it is observed that the loss caused by the stator is obvious, so the optimized stator structure [28] is selected in this paper. Through the efficiency iteration process shown in Fig. 2, the point where the overall efficiency matches the geometric losses is obtained. The final detailed geometric module provides the necessary information for the three-dimensional (3D) blade optimization stage. Moreover, the feasibility of each design scheme is addressed based on the selection criteria that comprise not only optimal operating ranges of the aerodynamic design, but also manufacturability and structural/vibration constraints. To obtain the real gas properties, TOPGEN is coupled to the REFPROP database by the National Institute of Standards and Technology (NIST). For SCO_2, TOPGEN gives access to the Span and Wagner equations of state (SW EoS) [29].

The design conditions for the input of the calculation model are listed in Table 1. After filtering the feasible data, a set of turbine parameter data is obtained as shown in Table 2. According to the geometric parameters after optimizing the design, the ANSYS-BladeGen module is adopted to construct the 3D model of the turbine stage part. The final calculation 3D model applied in the following simulation can

Table 1
The initial conditions of the calculation.

Parameter	Value
Power, W [kW]	500.00
Rotational speed, N [kRPM]	100.0
Inlet total temperature, T_{01} [K]	833.15
Inlet total pressure, P_{01} [MPa]	20.00
Mass flow rate, $\dot{m}$ [kg/s]	5.30
Pressure ratio (Total-Static), PR [–]	2.22
Flow coefficient, φ [–]	0.38
Head coefficient, ψ [–]	0.86

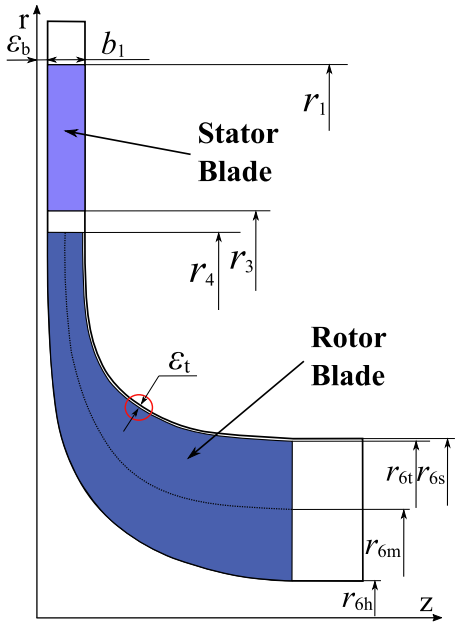

Fig. 3. Schematic diagram of the turbine meridian plane.

be seen in Fig. 1. Moreover, a meridional-plane projection of the stator and the rotor is illustrated in Fig. 3.

2.2. Numerical method and boundary conditions

The construction of the cycle system consumes vast labor power and financial resources, and the assembly of the test-rig is very costly. Hence, it is impractical to build a corresponding test-rig to adapt to the cycle system of different mixtures. Considering the above situation, the existing turbine model designed for pure CO_2 is selected to simulate the situations using different CO_2-based binary mixtures. In this study, the 3D steady and unsteady simulations are conducted by the ANSYS platform. ANSYS-BladeGen is used to build the 3D turbine model, and the structured mesh used in CFD simulation is generated through TurboGrid. Fig. 4 presents the mesh of the computation domain, which includes two nozzle passages and a single rotor passage. Since the existence of 0.1 mm tip clearance has a noticeable impact on the turbine flow performance, the grid at this position is refined.

ANSYS-CFX is employed to perform the numerical simulation. The boundary conditions of the designed RIT are the same as the design conditions, as shown in Table 1. The total pressure, the total temperature, and the absolute velocity direction are imposed as the stator inlet boundary conditions, whereas the static pressure is set as the rotor outlet boundary condition. The Mixing-Plane method between stator and rotor interfaces is set in the steady-state simulation for information exchange. Since using simplified passage model, the interfaces between passages are defined as periodic boundaries. The characteristics of turbine internal flow are complex, as separated flows and vortex mix

Table 2
Design parameters for turbine.

Rotor parameter	Value	Stator parameters	Value
Inlet radius, r_4 [mm]	31.63	Inlet radius, r_1 [mm]	41.91
Inlet blade height, b_4 [mm]	2.25	Blade height, b_1 [mm]	2.35
Inlet absolute flow angle, α_4 [°]	66.16	Outlet radius, r_3 [mm]	33.21
Inlet relative flow angle, β_4 [°]	−20.22	Stator installation angle, α_1[°]	56.00
Tip clearance, ε_t [mm]	0.10	Stator blade length, r_3 [mm]	15.00
Outlet hub radius, r_{6h} [mm]	9.49	Outlet absolute flow angle, α_3 [°]	65.08
Outlet shroud radius, r_{6s} [mm]	18.53	Outlet relative flow angle, β_3 [°]	67.56
Outlet hub angle, β_{6h} [°]	−38.29	Trailing edge thickness, t_3 [mm]	0.90
Outlet tip angle, β_{6t} [°]	−57.03	Stator blade number, Z_s [–]	20
Blade thickness, t_r [mm]	1.00		
Rotor blade number, Z_r [–]	13		

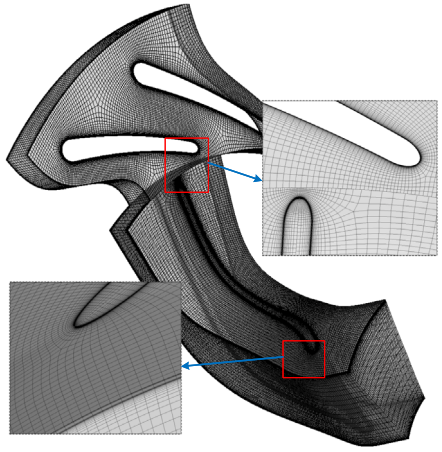

Fig. 4. Computational grid of SCO_2 RIT.

along the passage, resulting in highly turbulent flow. The losses are generated, due to the flow separation caused by gas impact on the leading edge, the shed vortex of the trailing edge, and the secondary flow caused by clearance leakage flow. Therefore, the turbulence model adopts the $k-\omega$ SST model, which is more accurate in predicting the flow with strong adverse pressure gradients. Moreover, no slip-wall boundary condition is employed on any solid wall. The convergence residual values of each physical quantity are marked as 10^{-5}. When the turbine operates under off-design conditions, the outlet pressure of the turbine is kept constant while the inlet pressure is changed, so as to fit the variable condition characteristics of the cycle [30].

2.3. CO_2-based binary mixtures

The NIST REFPROP database [26] is applied to obtain all thermophysical properties of working fluids. The properties of the working fluid are loaded into RGP tables and used in ANSYS CFX [31,32]. Moreover, the use of REFPROP to calculate the thermophysical properties of CO_2-based binary mixtures in cycle systems has been generally recognized [10–15]. Besides, the physical property data obtained by Xue et al. [33] through molecular dynamics (MD) simulation matched well with the NIST database. Therefore, it is a feasible option to combine the above two methods to apply the RIT simulation in this study. Due to the limitation of existing experimental data, NIST gives suggestions on the selection of pressure and temperature ranges of the various mixtures [34]. However, to assess a higher turbine inlet temperature, the selected temperature range is widened to 900 K. The extended temperature range can be obtained because fluids behave as ideal gases and their properties vary regularly with different pressures and temperatures. Meanwhile, the uncertainty of the prediction of high-temperature physical properties is difficult to discuss.

In this paper, an in-house python code is developed to obtain the physical properties of the working fluid from the NIST REFPROP database to generate RGP files for pure CO_2 and CO_2-based binary mixtures. The RGP table contains 9 physical properties of the mixture, such as the h, s, C_p, etc. With the tabulated physical properties supplied, ANSYS CFX can solve the governing equations by directly reading the physical data in these external tables. The established GERG 2008 EoS [34,35] is employed to calculate the properties of mixtures CO_2–N_2, CO_2–O_2, and CO_2–He. For CO_2–Kr and CO_2–Xe, the binary interaction parameters are automatically fitted for the multi-fluid models' calculations (Helmholtz-Energy-Explicit mixture models) [36]. The equation is based on multi-fluid approximations and is explicit in the Helmholtz free energy.

The mixture model is a specific basic equation in Helmholtz free energy a, with independent mixture variable density ρ, temperature T, and the vector $\bar{x}$ of molar composition. In the form of dimensionless Helmholtz free energy $\alpha = a/(RT)$, the equation is as follows:

$$\alpha(\delta,\tau,\bar{x}) = \alpha^o(\rho,T,\bar{x}) + \alpha^r(\delta,\tau,\bar{x}) \tag{1}$$

where $\delta = \rho/\rho_r$ and $\tau = T_r/T$. The ρ_r and T_r are the composition-dependent reducing functions for the mixture density and temperature, which are calculated by Eqs. (2) and (3). The function $a(\rho, T, \bar{x})$ is split into a part α^o, which represents the properties of ideal-gas mixtures at given values for ρ, T, and $\bar{x}$, and a part α^r, which takes into account the residual mixture behavior.

$$\frac{1}{\rho_r(\bar{x})} = \sum_{i=1}^{N} x_i^2 \frac{1}{\rho_{c,i}} + \sum_{i=1}^{N-1}\sum_{j=i+1}^{N} 2\,x_i\,x_j\,\beta_{v,ij}\,\gamma_{v,ij}\,\frac{x_i+x_j}{\beta_{v,ij}^2\,x_i+x_j}\,\frac{1}{8}\left(\frac{1}{\rho_{c,i}^{1/3}}+\frac{1}{\rho_{c,j}^{1/3}}\right)^3 \tag{2}$$

$$T_r(\bar{x}) = \sum_{i=1}^{N} x_i^2\,T_{c,i} + \sum_{i=1}^{N-1}\sum_{j=i+1}^{N} 2\,x_i\,x_j\,\beta_{T,ij}\,\gamma_{T,ij}\,\frac{x_i+x_j}{\beta_{T,ij}^2\,x_i+x_j}\,(T_{c,i}\,T_{c,j})^{0.5} \tag{3}$$

The binary parameters $\beta_{v,ij}$, $\beta_{T,ij}$, $\gamma_{v,ij}$, and $\gamma_{T,ij}$ are fitted to data for binary mixtures and dependent on each additive. $\rho_{c,i}$, $\rho_{c,j}$, $T_{c,i}$, and $T_{c,j}$ are critical parameters of the pure components.

To verify the accuracy of the physical properties of the working fluid in this study, the CO_2–Xe binary mixture is taken as an example. Fig. 5 shows the comparison of the mixture's isobaric specific heat capacity c_p calculated in this study with Xue's MD calculation results [33]. The line graph depicts the change of the c_p of the working fluid under the pressure of 15 MPa. The calculated results are similar to the MD simulation results, and these two groups of data can verify each other, which indicates that the physical properties of the supercritical fluid used in this study are credible.

2.4. Verification of computational mesh and property tables

To carry out the mesh independency study, 4 meshes with different resolutions are generated and marked with Mesh 1 to 4, as shown in Table 3. Comparing the turbine mass flow rate, $\dot{m}$, total to static efficiency, η_{t-s}, and total torque, M, the relative error between Mesh 3

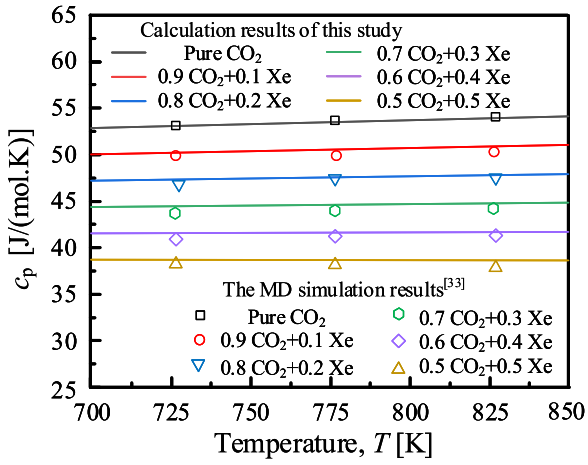

Fig. 5. The isobaric heat capacity, C_p, of CO_2–Xe binary mixtures as a function of temperatures, T, calculated by this study and MD at 15 MPa.

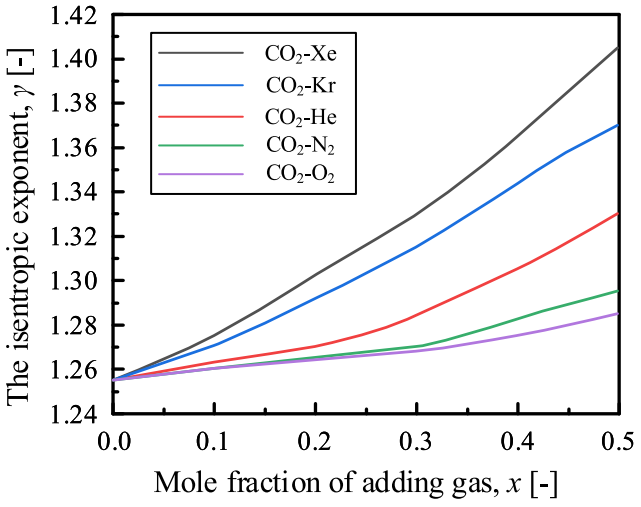

Fig. 6. Variation of mixtures isentropic exponent vs. the mole fraction of additives.

Table 3
Mesh independency study.

Mesh	Rotor cell number/×10⁴	Stator cell number/×10⁴	$\dot{m}$/[kg/s]	η_{t-s}/%	M(all blade)/[N m]
1	34.0	11.6	5.34	78.95	47.85
2	49.4	15.5	5.33	78.62	47.57
3	74.3	19.3	5.30	79.07	47.50
4	111.2	30.2	5.29	79.14	47.48

Table 4
Comparison of 1D design and simulation values of SCO_2 RIT.

Case	W/kW	η_{t-s}/%	$\dot{m}$/[kg/s]
1D TOPGEN results	500.00	79.02	5.30
3D CFD results with CO_2RK	496.78	79.07	5.30
3D CFD results with RGP table	498.25	79.05	5.29

and Mesh 4 for these parameters are 0.18%, 0.08% and 0.04%. These relative errors are quite limited, indicating that Mesh 3 has sufficient resolution for carrying out the following simulations. For the single passage model, the cell number of the stator is 193,000, and the cell number of the rotor is 743,000.

The data in the RGP tables are derived by setting the mole fraction of CO_2 to 1 and the mole fraction of the additive to 0 in the mixture composition. To study the independence of the RGP table to the resolution, 5 different RGP tables with different resolutions, 100 × 100, 200 × 200, 300 × 300, 400 × 400 and 500 × 500 are generated and applied in simulation. Considering the independence, stability, convergence, and accuracy of the simulation, RGP tables with a resolution of 400 × 400 are finally adopted in the following simulations.

Table 4 shows the comparison between the 3D numerical simulation results and the 1D results. The CFD simulation data are consistent with the TOPGEN design results, which manifests that the simulation process and the design process are mutually verified and explains the rationality of the RIT model. Furthermore, the simulation results based on RGP tables are close to those based on the Aungier-Redlich-Kwong cubic equation [37,38], demonstrating the accuracy of the RGP table resolution and the process of obtaining the mixture's physical properties.

3. Results and analysis

A 500 kW SCO_2 RIT is designed and discussed. Firstly, the turbine operated with various mixtures under a designed condition to explore its performance change. Then the mixture with a positive effect (enhance the turbine efficiency) is selected to compare the turbine performance under off-design conditions and explore the change of turbine operation range. Moreover, to further study the underlying reasons for the mixture's effects through simulations, the entropy change of the turbine stage passage is analyzed. Finally, the variation of turbine efficiency is calibrated by a transport characteristic, and the source of losses is revealed by loss breakdown, which provides a reference for optimizing the turbine to adapt to the specific cycle.

3.1. SCO_2 RIT with SCO_2-based binary mixtures at design point

CO_2-based binary mixtures with different components and mixing ratios are used to explore the influence of additives on the turbine performance. The selected mole fractions, x, of various additives are 0.5%, 1%, 5%, 10%, 20%, 30%, 40%, and 50%. Then the steady-state simulation is carried out under the design condition. The constant boundary condition at the stator inlet is set to 833.15 K and 20 MPa. At the rotor outlet, the static pressure maintains 9.009 MPa. The additive changes the thermodynamic and transport characteristics of the working fluid in the supercritical region, so it is necessary to use a parameter to calibrate the working fluid characteristics. Roberts et al. [39] suggested that the isentropic exponent, $\gamma = \frac{C_p}{C_v}$, is an important criterion of similarity in the performance of turbomachinery. Their study showed that the choking $\dot{m}$, the pressure ratio, and the isentropic efficiency of the compressors are all significantly affected by the changes in γ. Under the inspiration of Roberts's work, this study attempts to use γ as the parameter to calibrate the mixture characteristics for the following exploration of their influence on the RIT.

Through the comparison of γ of the CO_2-based mixtures for multiple state points, limited change can be found within the operating temperature range of RIT. So it can be considered that the specific mixture has a relatively stable γ in this interval. However, for different additives, the changes of the mixture γ are different with the increasing amount of the additives, as shown in Fig. 6. The introduction of xenon has the greatest effect on the thermal properties of CO_2, while nitrogen and oxygen have the smallest impact. In addition, the CO_2–He mixture γ growth rate, $\frac{\partial \gamma}{\partial x}$, increases with an increased x of helium. This phenomenon indicates that with the increase of x, the effect of adding helium tends to be more significant to the change of the CO_2 properties. Furthermore, the γ of the CO_2–Kr mixture increases almost linearly with the increase of x.

The variations of the RIT isentropic efficiency with different components and mixing ratios of the mixtures are shown in Fig. 7. As the variation of γ implies, the introduction of xenon has the largest

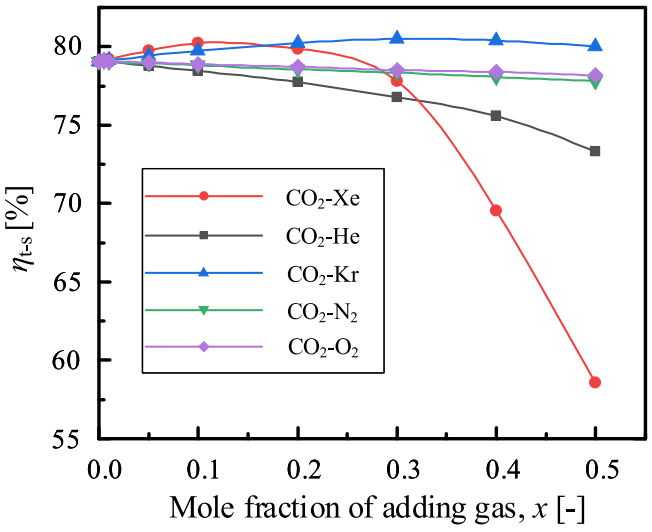

Fig. 7. Variation of RIT isentropic efficiency vs. the mole fraction of additives.

impact on turbine efficiency. With the increase of xenon amount, the efficiency shows a trend of first increase and then decrease, and the highest efficiency point appears at x about 10%. When x of xenon is higher than 20%, the turbine efficiency decreases rapidly. Contrary to adding xenon, the addition of krypton will increase the turbine efficiency. Nitrogen and oxygen are often considered to be inevitable impurity gases, but the effect on turbine efficiency is little when mixed in a small amount. Helium has been widely used in the applications of power conversion systems, such as the Gas Cooling High-Temperature Reactor. When helium is used as an additive, it has a negative effect on turbine efficiency. With the increase of x, the decline rate of turbine efficiency accelerates. In all, mixing an appropriate amount of krypton or a small amount of xenon into the working fluid can improve the turbine performance, while the other three additives negatively affect turbine operation.

To further analyze the influence of working fluid properties on turbine performance, the following research is carried out. Fig. 8 illustrates the variation curves of mixture ρ and turbine $\dot{m}$ as the mole fraction of additive changes under the design condition. The turbine $\dot{m}$ is closely related to the mixtures ρ when the CFD simulations are carried out with fixed geometry and inlet velocity. When a higher ρ of the mixture is used in the turbine, the operating $\dot{m}$ will decrease. On the contrary, a lower ρ of the mixture causes a higher $\dot{m}$. The ρ of the CO_2–Xe mixture deviates most from pure CO_2 with an increased x of xenon. Therefore, the change of $\dot{m}$ is the largest, resulting in the instability of turbine operation, which is manifested in the significant reduction of efficiency, as shown in Fig. 7. As a bioinert gas with low molecular weight, helium has low ρ and high kinematic viscosity, μ. It significantly reduces the working fluid ρ, making the $\dot{m}$ of the turbine decrease linearly. The shaft power of RIT depends on the $\dot{m}$ and the enthalpy levels of working fluid at the inlet and the outlet, shown in Eq. (4):

$$W_{tur} = m_g(h_1 - h_6) = m_g\,\eta_{tur}(h_1 - h_{6s})\ . \tag{4}$$

Turbine total to static isentropic efficiency can be calculated through:

$$\eta_{tur} = \eta_{t-s} = \frac{h_1 - h_6}{h_1 - h_{6s}}\ . \tag{5}$$

Then the total enthalpy difference between the inlet and outlet of the turbine is calculated. The variations of enthalpy difference and output power with the increased mole fractions of additives are shown in Fig. 9. The power output can be predicted by the enthalpy difference, while the $\dot{m}$ has a relatively small effect on the trend of the output power. The enthalpy difference decreases significantly with an increased amount of xenon and krypton, leading to a decrease in the turbine output power. The introduction of helium increases the enthalpy difference to the maximum extent. However, due to the decrease in $\dot{m}$, the final turbine power growth rate decreases. For the introduction of nitrogen and oxygen, the enthalpy differences between the turbine inlet and outlet dominate the rise of the output power. Furthermore, for the five additives in this paper, the mixture has little effect on the turbine performance when the x is less than 1%.

3.2. SCO_2 *RIT with* SCO_2*-based binary mixtures under off-design condition*

The above analysis shows that under the premise that the inlet and outlet boundary conditions of the turbine are constant, the influence of different additives on the turbine is obviously different, and the turbine performance also changes significantly with the amount of additives. The influence of mixtures on turbine performance under off-design conditions is further analyzed. In this section, only CO_2–Kr binary mixture is analyzed as it is the only helpful additive to improve turbine efficiency. Fig. 10 shows the efficiency curve of the off-design conditions when the turbine outlet pressure is constant and the inlet pressure is changed. When the additive's x is 1%, the mixtures have little effect on the variable operating conditions of the turbine, and the turbine highest efficiency point almost coincides with the operation using pure CO_2. However, with the increase in the amount of krypton, the deviation of the turbine performance curve under off-design conditions becomes larger. With an increased x of krypton, the highest point of turbine efficiency moves to the right, which is the direction of increasing inlet pressure. Moreover, the mixtures with higher amount of krypton show detrimental effects under the lower turbine inlet pressure. The above results indicate that the operational range of the turbine becomes narrow.

Fig. 11 shows the influence of different ratios of CO_2–Kr mixture on the turbine shaft power and $\dot{m}$ under variable working conditions. For the turbine shaft power in Fig. 11, the distribution is almost linear with respect to the inlet pressure when the mixing ratios change. The $\dot{m}$ demand increases with the increase of inlet total pressure, and the binary mixture with higher krypton x brings a greater growth rate in $\dot{m}$. On the one hand, with an increasing Kr amount and operating pressure, the working fluid ρ increases, resulting in a rise in $\dot{m}$. On the other hand, for a fixed turbine geometry, $\dot{m}$ depends mainly on pressure. A larger pressure drop accelerates the overall flow speed in the turbine so that $\dot{m}$ increases.

3.3. *Turbine stage losses analysis*

To understand the influence of mixtures on turbine performance more clearly, the overall loss of the turbine stage is studied. Fig. 12 depicts the entropy rise in the passage at different percentages of the blade spans when the RIT uses pure CO_2. The entropy growth rate fluctuates greatly in the middle and downstream part of the rotor passage, which is caused by the vortex generated through the tip clearance leakage flow. More separated flow and secondary flow in the channel lead to an increase in flow losses. Further, Fig. 13 shows the changes in the average entropy in the turbine stage passage under the different mixing ratios of nitrogen, xenon, helium, and krypton. The losses in the stator passage gradually decrease with the increase of the xenon x. However, the losses decrease at first and then increase in the rotor passage. When the x of xenon exceeds 20%, the stage losses increase sharply, indicating that the influence of mixtures on the turbine performance is intensified, and even affects its operation stability. According to the previous analysis, nitrogen and oxygen have similar effects on turbine performance, so this section only analyzes the influence of nitrogen on stage losses. Overall, nitrogen has a negative effect on the rotor turbine stage losses. The effect of the CO_2–Kr mixture is opposite to that of the CO_2–N_2 mixture, and the losses gradually decrease with

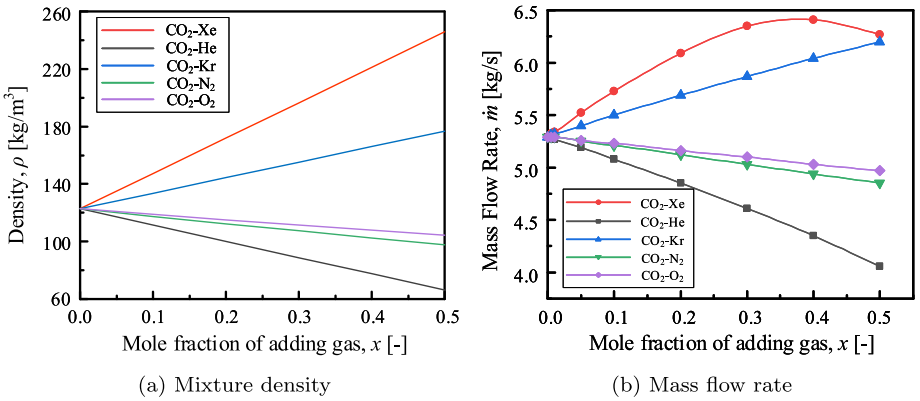

(a) Mixture density (b) Mass flow rate

Fig. 8. Variation of mixture density and RIT mass flow rate vs. the mole fraction of additives.

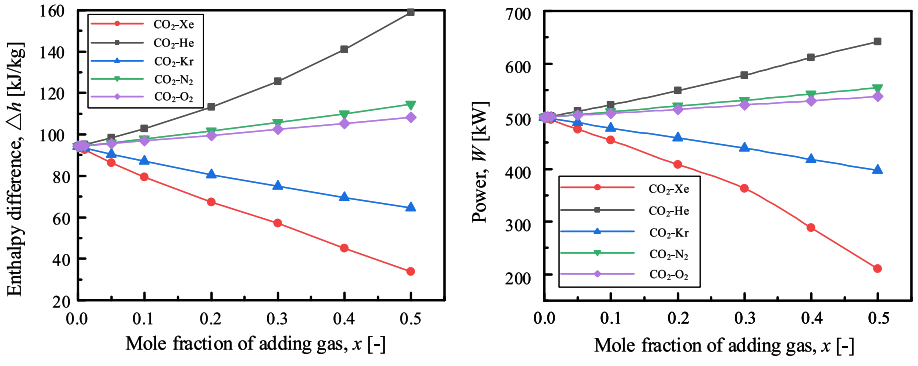

(a) Enthalpy at stator inlet (b) Shaft power

Fig. 9. Variation of mixture enthalpy at stator inlet and shaft power vs. the mole fraction of additives.

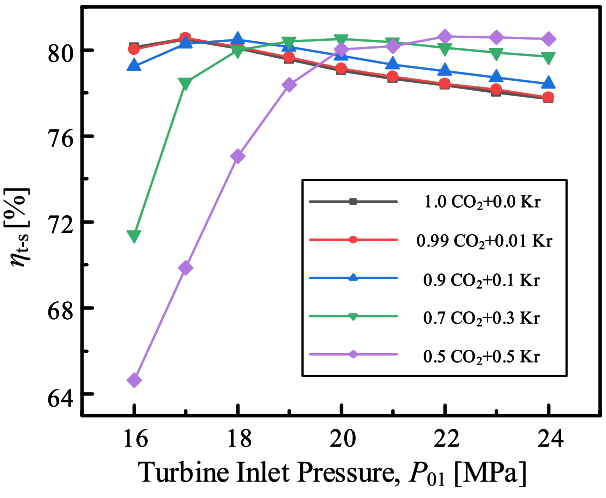

Fig. 10. Variation of the isentropic efficiency vs. the turbine inlet pressure.

the x of krypton increasing, which also explains why CO_2–Kr can improve turbine efficiency. The addition of helium also contributes to the increase in stage loss, and its negative effect is greater than that of nitrogen. There are two purposes for the investigation of the entropy change curve. One is to observe the relationship between efficiency and loss more intuitively. Another aspect is to reflect the prediction of turbine performance through CFD simulations. The entropy drop at the interface becomes obvious with the increase in helium amount, which indicates the uncertainty of steady-state simulation prediction.

For the steady-state simulation, the Stage model (Mixing-plane method) is used to exchange the information at the stator and rotor interface. The stage model performs a circumferential averaging of the fluxes at different bands on the interface. Then steady-state solutions are obtained in each reference frame. The stage averaging at the interface leads to a one-time numerical mixing loss, which is characterized by a sudden entropy rise. However, there is a sharp entropy drop at the interface when the helium x is larger than 20%, which is not logical. Hence, the entropy and Reynolds number at the interface when the x of helium is 1% and 50% are studied and shown in Fig. 14. The averaging effect is obvious when the amount is small, and the equivalent regions of entropy and Reynolds number (Re) show a banded distribution. When the amount of helium is relatively large, the average effect of entropy at the interface is unsatisfactory, especially at the trailing edge of the stator. It can be observed from the Re contours that the interface Re distribution is not regular, indicating that the information processing results may be inaccurate. To further reveal the strong unsteady characteristics under this condition, the next study is conducted.

The CO_2–He binary mixture with a 50% helium mole fraction is selected to conduct a detailed study. Fig. 15 shows the RIT stage losses under three different simulation settings. On the one hand, an information processing method of the interface called Frozen Rotor is used for steady-state simulation in this paper. Compared to the Mixing-plane, Frozen Rotor maps variables directly to the neighbor patch so that the computation requirement of steady-state simulation is reduced. However, the entropy value gradually tends to be consistent at the rotor passage center with the development of the main flow. Therefore, it can be considered that the steady-state simulation has a similar effect on the overall performance prediction of the turbine when using the two interfaces. On the other hand, when using the CO_2–He mixture at

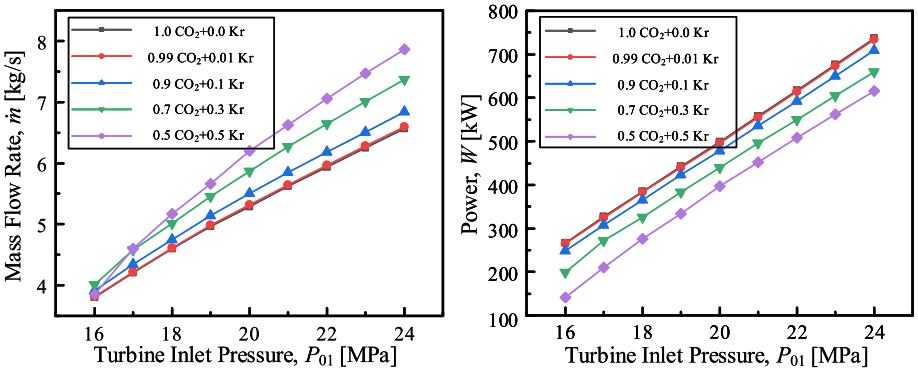

(a) Mass flow rate (b) Shaft power

Fig. 11. Variation of the shaft power and mass flow rate vs. the turbine inlet pressure.

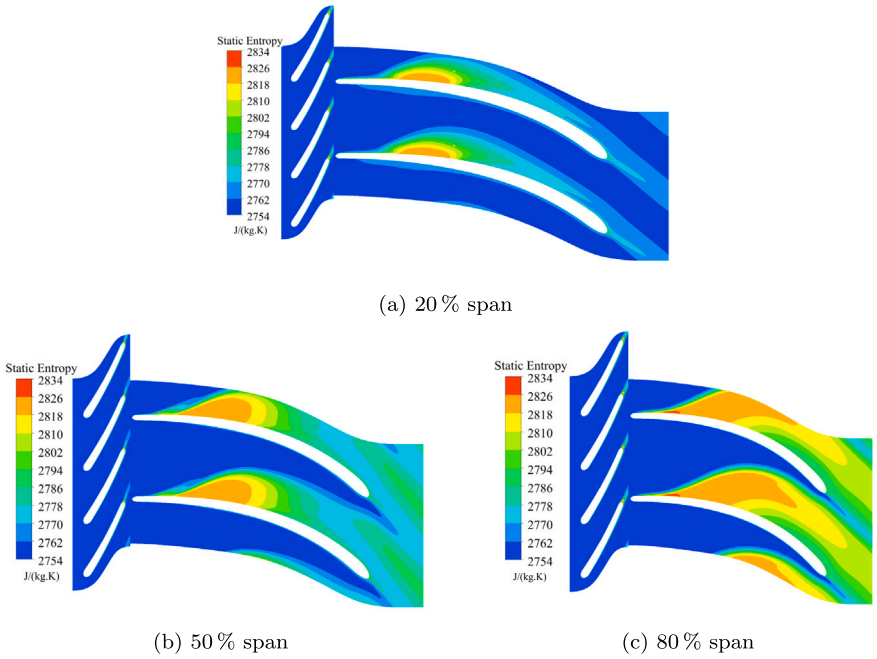

(a) 20 % span

(b) 50 % span (c) 80 % span

Fig. 12. Static entropy contours at different spans with pure CO_2.

a high helium amount, the steady-state simulation can hardly reach convergence. It is concluded that the unsteady characteristics of the turbine are strong, and the steady-state simulation cannot predict turbomachinery performance well. Then the transient simulation of the turbine under this working fluid is analyzed. Comparing the entropy increase between the steady-state and transient simulations in Fig. 15, the two performance predictions are significantly different. It is mainly reflected in the loss prediction produced by the interaction effect between the stator and rotor. Under the real situation (transient simulation), the entropy rise is obvious from the stator outlet to the rotor leading edge. However, the stage averaging between static and dynamic passages only accounts for the time average interaction effects. Even though the stage averaging assumes a sufficiently large physical mixing generated by the relative motion, the neglected transient interaction still plays an important role. This is because the ρ of the mixture has been greatly reduced at high helium amount, which is significant for small size and high-speed RITs. Then the turbine operation tends to be more unstable as the transient interaction between the stators and rotors intensified. Therefore, the turbine designed with pure CO_2 is no longer suitable for high mixing ratio CO_2–He mixtures.

3.4. Breakdown of losses

From the perspective of transport characteristics of the working fluids, the influence of the dynamic viscosity, μ, on the turbine stage losses are investigated in this section. Through the transport model calculation based on the thermophysical properties from REFPROP database, it can be found that different additives have variant levels of increase effect on the μ. The dynamic viscosity of the mixture obeys a states principle shown in Eq. (6) [40]:

$$\mu(T,\rho,\bar{x}) = \mu^*(T,\bar{x}) + \Delta\mu(T,\rho,\bar{x}) = \mu^*(T,\bar{x}) + \Delta\mu_0(T_0,\rho_0)F_\mu(T,\rho)\ , \quad (6)$$

where the superscript * denotes a dilute gas value, and the subscript $_0$ denotes a reference fluid value. F_μ is a mixture's factor that contains the use of mixing rules.

When nitrogen and oxygen are introduced as impurity gases with a slight amount, the change of μ is little, and the influence on the turbine performance can be ignored. The amount of helium also has a limited effect on the μ of the mixture, only reducing the ρ to a great extent. Therefore, the turbine efficiency deviates from the normal working condition after the $\dot{m}$ changes, which will cause larger losses. The addition of krypton and xenon has a great influence on

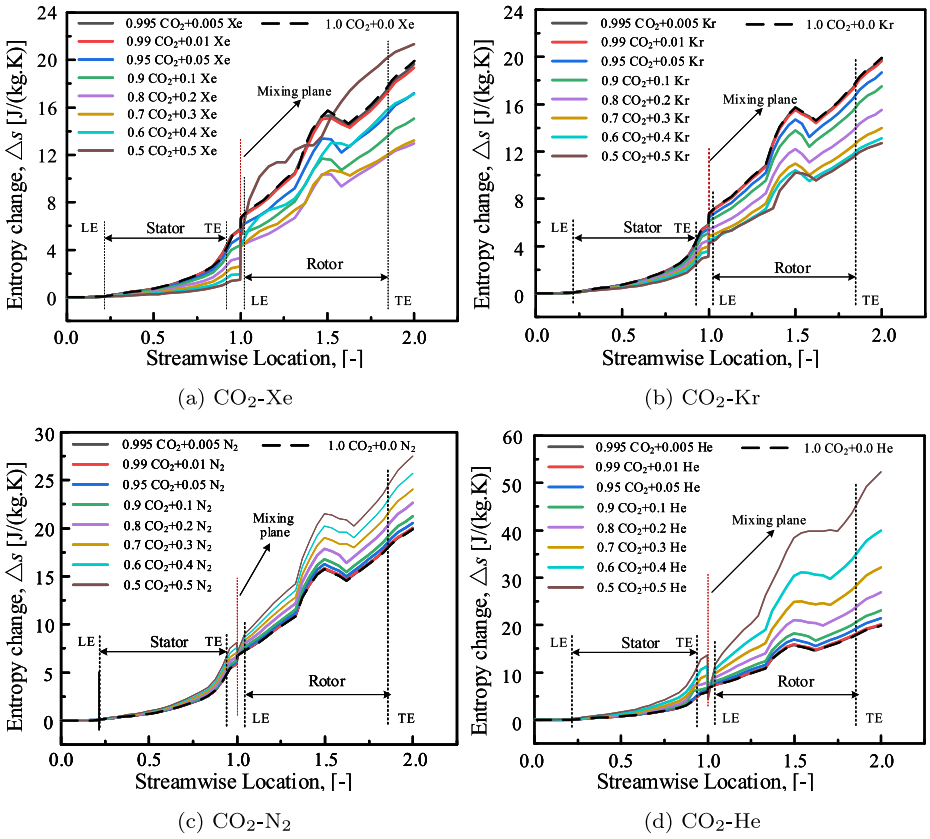

Fig. 13. Variation of the passage entropy change vs. the streamwise location.

the transport characteristics of CO_2, and the influence from xenon is more intense. The simulation results show that the working fluid pressure and temperature levels are in the range of 8 MPa to 20 MPa and 700 K to 835 K during turbine operation. As shown in Fig. 16, the μ of the mixtures under different mixing ratios are analyzed in combination with the turbine operation efficiency. For the binary mixtures of CO_2–Kr and CO_2–Xe, there is a reasonable μ range that makes the turbine efficiency higher than that by adopting pure CO_2. However, when the μ exceeds the reasonable range, it will have a negative effect on the turbine operation and reduce the turbine efficiency. The reason for this phenomenon is analyzed from the level of the turbine flow field. The Mach number contours of the 50% blade span under the different amounts of krypton are obtained, as shown in Fig. 17. The local low Mach number region begins to appear at the blade inlet pressure side, which is unfavorable to the normal condition, seriously hindering the output work of the turbine. Therefore, when substances similar to krypton and xenon are added, the appropriate amount can ensure the μ of the mixture in a reasonable range so that conducive to improving the turbine performance.

The cause of turbine loss has been preliminarily analyzed, but the exploration of the loss mechanism of the CO_2-based mixture turbine is not detailed enough. Therefore, to assess the performance of the turbine stage when CO_2-based mixture is applied, a loss breakdown study is performed. The purpose of this loss breakdown is twofold: firstly, to clarify the difference in the loss mechanism of SCO_2 RITs between using pure CO_2 and mixtures; secondly, to seek high loss regions to inform future preliminary design methods for the design of efficient turbomachinery. In this section, the CO_2–Kr mixture is used as an example. To study loss mechanism, the way to distinguish different losses are presented. Entropy loss is determined following the method of Wheeler and Ong [41,42]. Profile and trailing edge losses are determined as the entropy rise over each component resulting from the blade boundary layer and trailing edge losses (i.e., by setting a slip-wall on the blade walls). Endwall and secondary flow losses are determined as the entropy rise over each component caused by viscous endwall effects and induced secondary flows (i.e., by setting a slip-wall on the shroud and hub surfaces, which also prevents in large part the development of secondary flows). Tip clearance loss is calculated as the proportional entropy rise on the rotor due to the existence of tip clearance. Mixing loss is determined from the entropy rise across the mixing-plane in the steady CFD predictions. All these procedures can be done by adjusting the CFD simulations.

Fig. 18 shows a breakdown of the different contributions to losses from the turbine stage passage. Tip leakage loss decreases with the increase of krypton amount. It can be explained that the dynamic viscosity μ of the mixtures increases with the increase of the krypton x. In the meantime, smaller tip clearance is more sensitive to the change of transport characteristics of the working fluid. As a result, the tip clearance leakage decreases, and losses accordingly decrease. The loss reduction caused by the rotor section is obvious, which is assumed to be related to the decrease of the flow Re. An increase in the μ of the mixtures reduces the overall Re of the fluid flow. Therefore, the decrease in turbulence intensity will mitigate the flow separation. Moreover, the losses caused by the stator passage cannot be ignored compared with the rotor passage. Most of the loss models in the 1D preliminary design now focus on the rotor losses of the turbine, such as incidence loss, passage loss, tip clearance loss, and exit energy loss. However, limited attentions are focused on modeling of the stator losses. With the increase of the krypton x, the endwall and secondary flow losses in the stator are reduced, but the stator profile and trailing edge losses are gradually increased. Therefore, the efficiency improvement of the CO_2–Kr mixture is mainly due to the reduction of the tip clearance loss and the endwall and secondary flow losses of the passage.

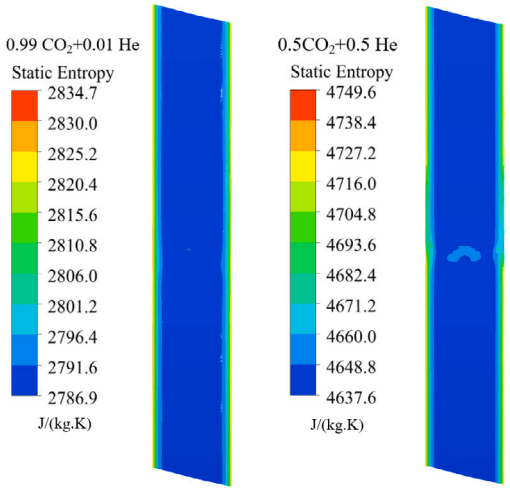

(a) Static entropy contours of the interface

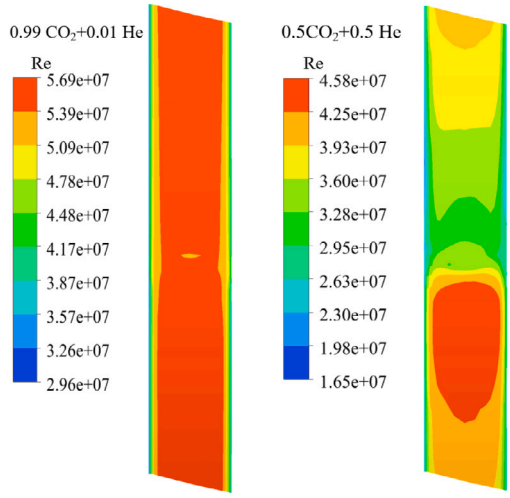

(b) Reynolds number contours of the interface

Fig. 14. Entropy and Reynolds number contours when the mole fraction of helium is 1% and 50%.

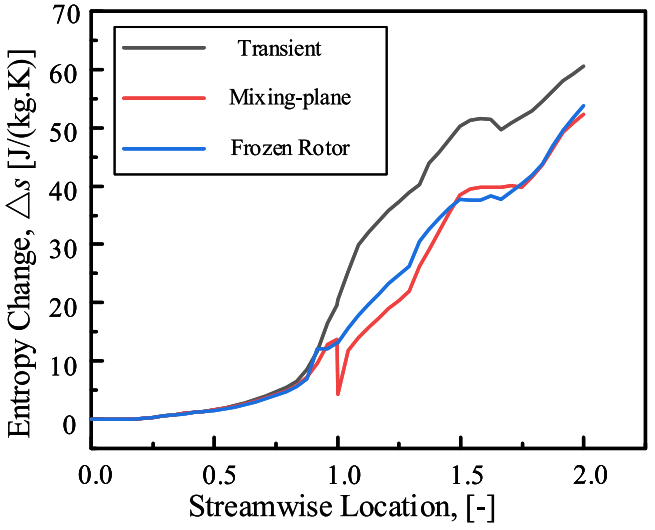

Fig. 15. The passage entropy change vs. the streamwise location under three different settings.

4. Conclusion

In this study, a 500 kW CO_2 radial-inflow turbine is designed and demonstrated. The effects of different additives (N_2, O_2, helium, xenon, and krypton) on the turbine performance are analyzed. Real gas properties of pure CO_2 and CO_2-based mixtures are accurately encoded for numerical simulation. Computational fluid dynamics simulations are carried out to explore the turbine performance and loss mechanism when using CO_2-based mixtures. At last, the loss breakdown analysis is investigated to illustrate the components of stage overall loss. The main conclusions are as follows:

(1) **Additives have different effects on turbine performance.** According to the calibration of thermodynamic properties by isentropic exponent γ, xenon, krypton, and helium have a great influence on the turbine. The small amount of xenon or appropriate amount of krypton added into the mixtures will increase the turbine efficiency, but reduce the turbine output power as the enthalpy differences dropped. However, helium behaves opposite to krypton and xenon. Nitrogen and oxygen, often introduced as inevitable impurity gas, bring a slightly negative impact.

(2) **The off-design performance and robust analysis of SCO_2 turbines under different mixtures are studied.** With the increase of krypton amount, the high-efficiency point moves toward the direction of higher inlet pressure, and the RIT performance deteriorates gradually under the low inlet pressure, indicating that the operation adaptation range of the turbine becomes narrow. The density of the CO_2–He mixtures is greatly reduced compared with the pure CO_2 density when the mole fraction of helium is high. Through the steady and transient simulations, it is assumed that the turbine designed with pure CO_2 is no longer suitable for the mixtures with high mole fraction helium.

(3) **The stage loss is analyzed detailedly with different mixtures, a properly dynamic viscosity range is proposed, and the loss breakdown analysis is also presented.** As the additive mole fraction increases, nitrogen and helium increase the entropy acceleratedly, while krypton increases the entropy hinderingly. Moreover, the total loss decrease at first and then increase with the increase of the xenon amount. A properly dynamic viscosity range is proposed so that the turbine can reach a high efficiency when the dynamic viscosity of the working fluids is in this range. Adding a predefined amount of rare gases, such as xenon and krypton, can change the dynamic viscosity of the mixtures into this range. The loss breakdown study is performed with the CO_2–Kr mixture, which indicates that the introduction of krypton can reduce tip clearance loss and end-wall and secondary flow losses. Moreover, the loss generated in the stator is significant.

In the future, it is suggested that full-scale turbine design procedures using different SCO_2-based mixtures should be explored. Also, a full robust examination of SCO_2-based mixture turbines based on γ and off-design conditions should be carried out. More important, as the compressor inlet condition is close to the CO_2 critical point, it is worth examining the performance of SCO_2 compressors operating with different CO_2-based mixtures. In addition, experimental and CFD comparisons should be performed for SCO_2 turbomachinery applications.

In all, the research carried out in this study will eventually benefit the SCO_2 power cycle community, and will contribute to the application of advanced power cycles.

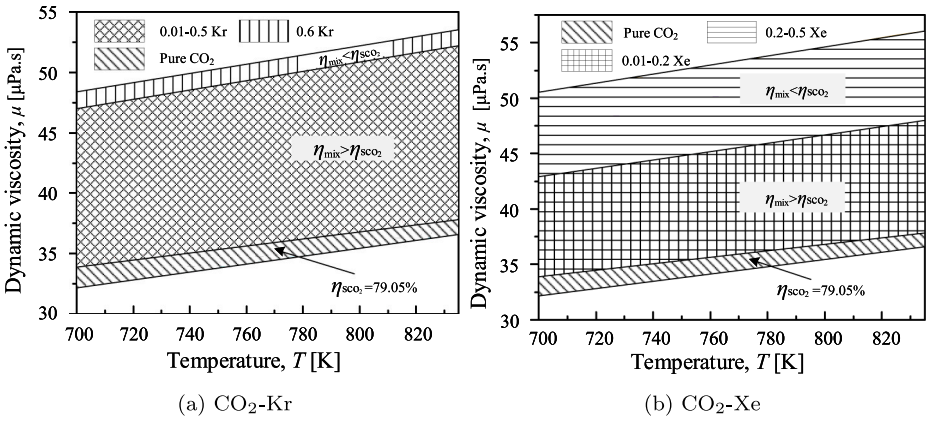

Fig. 16. Variation of the dynamic viscosity vs. the temperature.

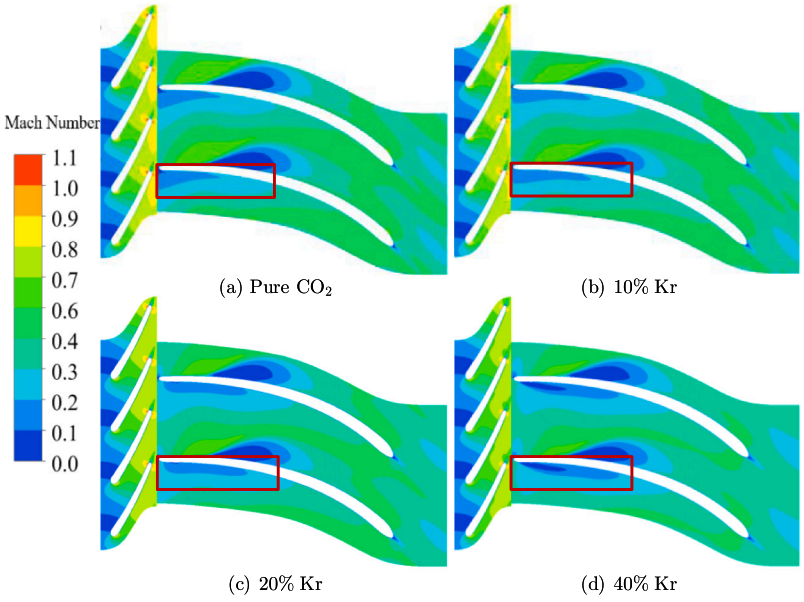

Fig. 17. Mach number contours of the turbine with different krypton mole fraction.

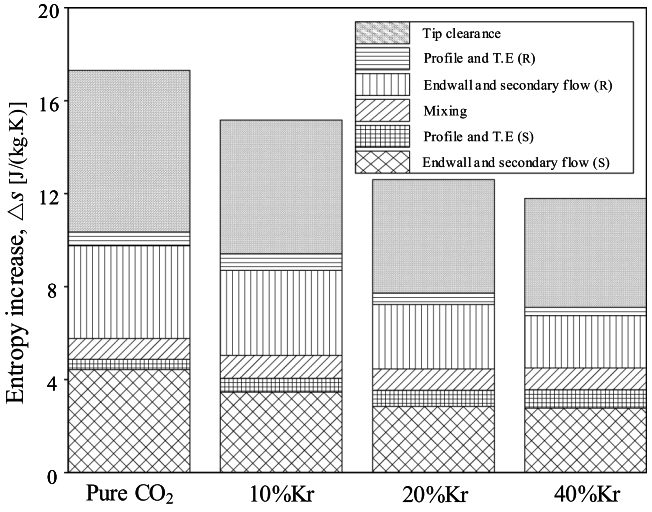

Fig. 18. Breakdown of predicted losses.

CRediT authorship contribution statement

Yueming Yang: Investigation, Conceptualization, Methodology, Software, Writing – original draft. **Xurong Wang:** Conceptualization. **Kamel Hooman:** Conceptualization. **Kuihua Han:** Conceptualization. **Jinliang Xu:** Formal analysis. **Suoying He:** Conceptualization. **Jianhui Qi:** Supervision, Funding acquisition, Methodology, Writing – review & editing.

Declaration of competing interest

The authors declare that they have no known competing financial interests or personal relationships that could have appeared to influence the work reported in this paper.

Data availability

The data that has been used is confidential.

Acknowledgments

The authors gratefully acknowledge the support of the National Natural Science Foundation of China (Grant No: 52106049), the Natural Science Foundation of Shandong Province, China (ZR2021ME118, ZR2020QE191), the Natural Science Foundation of Jiangsu Province, China (BK20210113), the Beijing Natural Science Foundation, China (3222048), and the Young Scholars Program of Shandong University, China (31380089964175).

References

[1] Buongiorno J, Parsons JE, Petti DA, Parsons J. The future of nuclear energy in a carbon-constrained world. 2019.
[2] Dostal V, Driscoll MJ, Hejzlar P. A supercritical carbon dioxide cycle for next generation nuclear reactors. 2004.
[3] Zare V, Hasanzadeh M. Energy and exergy analysis of a closed Brayton cycle-based combined cycle for solar power tower plants. Energy Convers Manage 2016;128:227–37.
[4] Le Moullec Y. Conceptual study of a high efficiency coal-fired power plant with CO_2 capture using a supercritical CO_2 Brayton cycle. Energy 2013;49:32–46.
[5] Feher EG. The supercritical thermodynamic power cycle. Energy Convers 1968;8(2):85–90.
[6] Angelino G. Real gas effects in carbon dioxide cycles, vol. 79832. American Society of Mechanical Engineers; 1969.
[7] Al-Sulaiman FA, Atif M. Performance comparison of different supercritical carbon dioxide Brayton cycles integrated with a solar power tower. Energy 2015;82:61–71.
[8] Wang X, Wang J, Zhao P, Dai Y. Thermodynamic comparison and optimization of supercritical CO_2 Brayton cycles with a bottoming transcritical CO_2 cycle. J Energy Eng 2016;142(3):4015028.
[9] Sun E, Xu J, Li M, Li H, Liu C, Xie J. Synergetics: The cooperative phenomenon in multi-compressions S-CO_2 power cycles. Energy Convers Manage 2020;7:100042.
[10] Jeong WS, Lee JI, Jeong YH. Potential improvements of supercritical recompression CO_2 Brayton cycle by mixing other gases for power conversion system of a SFR. Nucl Eng Des 2011;241(6):2128–37.
[11] Jeong WS, Jeong YH. Performance of supercritical Brayton cycle using CO_2-based binary mixture at varying critical points for SFR applications. Nucl Eng Des 2013;262:12–20.
[12] Hu L, Chen D, Huang Y, Li L, Cao Y, Yuan D, Wang J, Pan L. Investigation on the performance of the supercritical Brayton cycle with CO_2-based binary mixture as working fluid for an energy transportation system of a nuclear reactor. Energy 2015;89:874–86.
[13] Vesely L, Dostal V, Stepanek J. Effect of gaseous admixtures on cycles with supercritical carbon dioxide. In: Turbo expo: Power for land, sea, and air, vol. 49873. American Society of Mechanical Engineers; 2016, V009T36A016.
[14] Vesely L, Dostal V. Effect of multicomponent mixtures on cycles with supercritical carbon dioxide. In: Turbo expo: Power for land, sea, and air, vol. 50961. American Society of Mechanical Engineers; 2017, V009T38A016.
[15] Guo J-Q, Li M-J, He Y-L, Xu J-L. A study of new method and comprehensive evaluation on the improved performance of solar power tower plant with the CO_2-based mixture cycles. Appl Energy 2019;256:113837.
[16] Bonalumi D, Lasala S, Macchi E. CO_2-$TiCl_4$ working fluid for high-temperature heat source power cycles and solar application. Renew Energy 2020;147:2842–54.
[17] Crespi F, de Arriba PR, Sánchez D, Ayub A, Di Marcoberardino G, Invernizzi CM, Martínez G, Iora P, Di Bona D, Binotti M, et al. Thermal efficiency gains enabled by using CO_2 mixtures in supercritical power cycles. Energy 2022;238:121899.
[18] Morosini E, Manzolini G, Di Marcoberardino G, Invernizzi C, Iora P. Investigation of CO_2 mixtures to overcome the limits of sCO_2 cycles. In: 76th Italian national congress ATI (ATI 2021), vol. 312. 2021, p. 08010–9.
[19] Invernizzi CM, van der Stelt T. Supercritical and real gas Brayton cycles operating with mixtures of carbon dioxide and hydrocarbons. Proc Inst Mech Eng, A 2012;226(5):682–93.
[20] Wu Y, Bai Y, Song Y, Huang Q, Zhao Z, Hu L. Development strategy and conceptual design of China lead-based research reactor. Ann Nucl Energy 2016;87:511–6.
[21] Qi J, Reddell T, Qin K, Hooman K, Jahn IH. Supercritical CO_2 radial turbine design performance as a function of turbine size parameters. J Turbomach 2017;139(8).
[22] Zhou A, Song J, Li X, Ren X, Gu C. Aerodynamic design and numerical analysis of a radial inflow turbine for the supercritical carbon dioxide Brayton cycle. Appl Therm Eng 2018;132:245–55.
[23] Zhou K, Wang J, Xia J, Guo Y, Zhao P, Dai Y. Design and performance analysis of a supercritical CO_2 radial inflow turbine. Appl Therm Eng 2020;167:114757.
[24] Allison T, Moore J, Pelton R, Wilkes J, Ertas B. Turbomachinery. In: Brun K, Friedman P, Dennis R, editors. Fundamentals and applications of supercritical carbon dioxide (SCO_2) based power cycles. The Officers' Mess Business Centre, Royston Road, Duxford, CB22 4QH, United Kingdom: Woodhead Publishing; 2017, p. 147–215.
[25] Cho SK, Lee J, Lee JI, Cha JE. S-CO_2 turbine design for decay heat removal system of sodium cooled fast reactor. In: Turbo expo: Power for land, sea, and air, vol. 49873. American Society of Mechanical Engineers; 2016, V009T36A006.
[26] Lemmon E, Huber M, McLinden M. NIST standard reference database 23: Reference fluid thermodynamic and transport properties-REFPROP, version 9.1. 2013, URL https://tsapps.nist.gov/publication/get_pdf.cfm?pub_id=912382.
[27] Ventura CA, Jacobs PA, Rowlands AS, Petrie-Repar P, Sauret E. Preliminary design and performance estimation of radial inflow turbines: an automated approach. J Fluids Eng 2012;134(3).
[28] Qi J. Simulation tools and methods for supercritical carbon dioxide: Development and application on open-source code. Springer Singapore; 2022.
[29] Span R, Wagner W. A new equation of state for carbon dioxide covering the fluid region from the triple-point temperature to 1100 K at pressures up to 800 MPa. J Phys Chem Ref Data 1996;25(6):1509–96.
[30] Wang X, Li X, Li Q, Liu L, Liu C. Performance of a solar thermal power plant with direct air-cooled supercritical carbon dioxide Brayton cycle under off-design conditions. Appl Energy 2020;261:114359.
[31] Odabaee M, Sauret E, Hooman K. CFD simulation of a supercritical carbon dioxide radial-inflow turbine, comparing the results of using real gas equation of estate and real gas property file. In: Applied mechanics and materials, vol. 846. Trans Tech Publ; 2016, p. 85–90.
[32] Lv G, Yang J, Shao W, Wang X. Aerodynamic design optimization of radial-inflow turbine in supercritical CO_2 cycles using a one-dimensional model. Energy Convers Manage 2018;165:827–39.
[33] Xue J, Nie X, Du Z, Li H-R, Zhao L, Zhu Y, Wang J. Molecular dynamics investigation on isobaric heat capacity of working fluid in supercritical CO_2 Brayton cycle: Effect of trace gas. J CO_2 Util 2022;55:101790.
[34] Kunz O, Klimeck R, Wagner W, Jaeschke M. The GERG-2004 wide-range equation of state for natural gases and other mixtures. 2007.
[35] Kunz O, Wagner W. The GERG-2008 wide-range equation of state for natural gases and other mixtures: an expansion of GERG-2004. J Chem Eng Data 2012;57(11):3032–91.
[36] Bell IH, Lemmon EW. Automatic fitting of binary interaction parameters for multi-fluid Helmholtz-energy-explicit mixture models. J Chem Eng Data 2016;61(11):3752–60.
[37] Redlich O, Kwong JN. On the thermodynamics of solutions. V. An equation of state. Fugacities of gaseous solutions. Chem Rev 1949;44(1):233–44.
[38] Augnier R, Fast A. Accurate real gas equation of state for fluid dynamics analysis applications. J Fluids Eng 1995;117:277–81.
[39] Roberts SK, Sjolander SA. Effect of the specific heat ratio on the aerodynamic performance of turbomachinery. 2005.
[40] Chichester JC, Huber ML. Documentation and assessment of the transport property model for mixtures implemented in NIST REFPROP (Version 8.0). US Department of Commerce, Technology Administration, National Institute of ...; 2008.
[41] Wheeler AP, Ong J. A study of the three-dimensional unsteady real-gas flows within a transonic ORC turbine. In: Turbo expo: Power for land, sea, and air, vol. 45660. American Society of Mechanical Engineers; 2014, V03BT26A003.
[42] Keep JA, Jahn IH. Numerical loss investigation of a small scale, low specific speed supercritical CO_2 radial inflow turbine. J Eng Gas Turbines Power 2019;141(9).